American Mineralogist, Volume 91, pages 880–893, 2006

Direct determination of cation site occupancies in natural ferrite spinels by $L_{2,3}$ X-ray absorption spectroscopy and X-ray magnetic circular dichroism

CAROLYN I. PEARCE,[1,*] C. MICHAEL B. HENDERSON,[1,2] RICHARD A.D. PATTRICK,[1] GERRIT VAN DER LAAN,[2] AND DAVID J. VAUGHAN[1]

[1]School of Earth, Atmospheric and Environmental Sciences and Williamson Research Centre for Molecular Environmental Science, The University of Manchester, Manchester M13 9PL, U.K.
[2]Synchrotron Radiation Department, CCLRC Daresbury Laboratory, Warrington WA4 4AD, U.K.

ABSTRACT

Cation distributions in natural ferrite spinels, some containing large amounts of Mg, Ti, Mn, and Zn, have been investigated using the element-, site-, and symmetry-selective spectroscopic techniques of $L_{2,3}$ X-ray absorption spectroscopy (XAS) and X-ray magnetic circular dichroism (XMCD). By comparing XMCD data with calculated spectra, the site occupancies of the Fe cations have been determined. From the analysis of natural ferrite spinels with formulae very close to that of pure magnetite (Fe_3O_4), a standard XMCD spectrum for natural magnetite is proposed. Magnetites with small numbers of cation vacancies due to oxidation (solid solutions with maghemite, γ-Fe_2O_3) show that all the vacancies occur in octahedral sites. Ti $L_{2,3}$ XAS of oxidized Ti-bearing magnetites (hereafter referred to titanomagnetites) shows that Ti is tetravalent occurring on the octahedral site with $10Dq$ ~2eV; Fe $L_{2,3}$ XMCD spectra indicate that the vacancies occur in both tetrahedral and octahedral sites. Mn $L_{2,3}$ XAS of the Mn-rich ferrite spinels shows that Mn is predominantly ordered onto the tetrahedral site with an Mn^{2+}:Mn^{3+} ratio of 0.85:0.15. Mn- and Zn-rich ferrite spinels have an excess of cations over 3.0 per 4-oxygen formula unit. The sign of the XMCD for Mn corresponds to a parallel alignment of the Mn moments with the Fe^{3+} moments in the tetrahedral sublattice.

This work demonstrates clearly that combined XAS and XMCD provides direct information on the distribution of multivalent cations in chemically complex magnetic spinels.

Keywords: Analysis, chemical (mineral), natural ferrite spinel, magnetite, major and minor elements, magnetic properties, order-disorder, site vacancies in natural ferrite spinel, XAS (XMCD), XRD data, microprobe analysis, Fe^{2+}/Fe^{3+} ratio, cation distribution

INTRODUCTION

Magnetite ($Fe^{3+}_2Fe^{2+}O_4$) is the most abundant member of the spinel group of minerals. It is present throughout the Earth's crust and uppermost mantle and is the main contributor to rock magnetism (O'Reilly 1994). Fe^{2+} and Fe^{3+} in natural magnetite can be replaced by other metallic cations, often with the same charge and similar ionic radius, to form substitutional series (Fe-bearing spinels are called ferrite spinels). A wide range of stoichiometries occurs naturally, e.g., titanomagnetite $Fe^{3+}(Fe^{2+},Fe^{3+},Ti^{4+})_2O_4$, franklinite $(Zn^{2+},Mn^{2+})(Fe^{3+},Mn^{3+})_2O_4$, magnesioferrite $Mg^{2+}Fe^{3+}_2O_4$, and jacobsite $(Mn^{2+},Fe^{2+})(Mn^{3+},Fe^{3+})_2O_4$; these form under a variety of conditions including magmatic, metamorphic, metasomatic, and hydrothermal.

Spinels are among the most important ferrimagnetic materials for industrial applications, including data storage, transformers, and antennae (Smit and Wijn 1959). The magnetoresistive properties of spinels have been of recent interest in the area of spin electronics (Coey et al. 1998). According to band theory, Fe_3O_4 is a half-metal above the Verwey transition temperature T_V (~120 K), i.e., its minority-spin electrons are conducting, whereas the majority-spin electrons are insulating. Below T_V, charge-ordering of the octahedral Fe site has been suggested from refinements of X-ray and neutron diffraction data (Wright et al. 2001), implying that the 3*d* electrons have a strongly localized character. The latter has been confirmed by X-ray magnetic circular dichroism (XMCD), giving an orbital magnetic moment of 0.65 μ_B per Fe_3O_4 formula unit (Huang et al. 2004), and hence no indication for a quenched moment, as in itinerant systems. In addition, research into the properties of natural ferrite spinels is of petrological and mineralogical interest because their intracrystalline cation ordering provides petrogenetic information on the temperature and oxygen fugacity of mineral formation (Buddington and Lindsley 1964; Frost 1991a, 1991b).

Analysis of cation distribution in the structures of natural spinels is complex due to difficulties in assigning the cations to the octahedral and tetrahedral sites. Accurate determination of Fe^{3+}:Fe^{2+} concentration in natural spinels is also problematic. Therefore, the site occupancies of cations in spinels tend to be studied using a combination of several complementary methods. These include X-ray and neutron diffraction, which can be used to probe cation ordering in minerals based on the difference in scattering properties of the elements present in the different sites. Using these techniques, the cation site occupancies can only be determined unambiguously for binary mixtures and they are not well suited to the analysis of chemically complex

* E-mail: carolyn.pearce@manchester.ac.uk

natural spinels. However, the cation distribution between the tetrahedral and octahedral sites has been modeled through a minimization program relating refined cation-oxygen distances to the cell parameter and oxygen coordinate for chemically complex minerals of known chemical composition (Carbonin et al. 1996). Iron (^{57}Fe) Mössbauer spectroscopy is a particularly powerful probe of the oxidation state, coordination, covalency, and magnetic ordering of iron atoms in solids that has been widely applied to minerals, including spinels (O'Neill et al. 1992; Roelofsen et al. 1992; Carbonin et al. 1996). However, Mössbauer spectroscopy is unable to distinguish the octahedral Fe ions by their oxidation state.

It has been demonstrated that $L_{2,3}$-edge XAS is an effective site and valency probe for chemically complex minerals containing 3*d* metals, which provides information that cannot be obtained as easily, or as reliably, in any other way (Cressey et al. 1993; Henderson et al. 1994; Schofield et al. 1995). XMCD, obtained using the difference in *L*-edge XAS for opposite magnetization, can also be used to provide a clear distinction between the different oxidation states and sub-lattice positions in magnetic materials. In this paper, the unique element-, valence-, and site-specific XAS and XMCD techniques have been used to study natural magnetite and titanomagnetite samples. XAS and XMCD spectra, along with compositional information and XRD data for 10 representative samples are presented and a "standard" XMCD spectrum for natural magnetite is proposed.

Spinel structural relations and applicability of XMCD

In spinels, the oxygen anions form a face-centered cubic close-packed array, in which the cation site occupation factor is ¼ for the tetrahedral sites (A sub-lattice) and ½ for the octahedral sites (B sub-lattice) (Fig. 1). The A and B sub-lattices are usually occupied by metal cations with different valencies, reflected mainly in the ratio M^{2+}:M^{3+} (1:2). The coordination of transition metal ions in the spinel structure can be predicted from crystal field theory, which relates the *d* electron configuration of the transition metal ion, and hence its relative stability (expressed in terms of crystal field stabilization energy, CFSE), to the symmetry of the surrounding ligands, in this case O^{2-} (Burns 1993). The spinel structure, in which the key variable parameters are the unit-cell edge and the positional parameter for oxygen, allows significant differences in cation distributions, leading to normal, $(M^{2+})^{A}(M^{3+}M^{3+})^{B}O_4$ or inverse, $(M^{3+})^{A}(M^{2+}M^{3+})^{B}O_4$ spinel structures. Intermediate cation distributions may be described using an inversion parameter (*i*), namely $(M^{2+}_{1-i}\,M^{3+}_{i})^{A}(M^{2+}_{i}\,M^{3+}_{2-i})^{B}O_4$, with $i = 0$ for a totally normal spinel and $i = 1$ for a completely inverse spinel. A fully disordered spinel structure occurs when $i = 2/3$ (Lindsley 1991; Lucchesi et al. 1999).

In a normal spinel, site preference is determined according to CFSE with the fourfold-coordinated A sites occupied by divalent ions and the sixfold-coordinated B sites occupied by trivalent ions. However, in end-member magnetite (Fe_3O_4), the Fe^{3+} has a much stronger preference for the smaller A site, perhaps due to its tendency to form hybrid sp^3 bonds (Goodenough and Loeb 1955), relegating the Fe^{2+} ion and the other Fe^{3+} ions to the B sites. Fe_3O_4 is thus an inverse spinel.

An important method for obtaining crystal field splittings, and therefore the crystal field stabilization energy, is by measurement of the absorption spectra of the transition metal ion. The $L_{2,3}$ XAS spectrum is due to electric-dipole transitions from a $3d^n$ ground state to the $2p^5 3d^{n+1}$ final states. The spectral line shapes of XAS are highly sensitive to the details of the ground state, and carry the signature of the atomic terms involved in the ground state, as demonstrated by Thole et al. (1985). The reason for these distinct spectral differences is that the dipole selection rules are very restrictive, thereby limiting the number of final states that can be reached from the ground state, therefore allowing a characterization of the latter. However, to apply these techniques, multiplet structure calculations involving atoms with more than one open shell must be employed. Such calculations have now become standard (Cowan 1981).

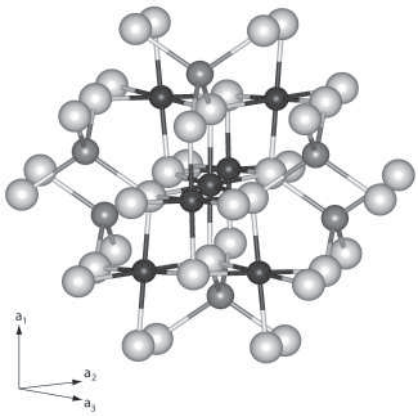

Figure 1. The spinel structure showing the octahedral cation sites (small black spheres), the tetrahedral cation sites (small dark gray spheres), and the oxygen anions (large light gray spheres) after Pattrick et al. (2002). (Structure created using the programs Cerius^2 and Weblab Life, Molecular Simulations Inc.)

End-member magnetite is a ferrimagnetic semi-conductor at room temperature with a Curie temperature of 850 K: the two different cation sites in the structure form two interpenetrating magnetic sublattices. The spin arrangement can be written as $(Fe^{3+}\downarrow)^{A}[Fe^{3+}\uparrow\ Fe^{2+}\uparrow]^{B}\ O_4$ where the square brackets indicate the octahedral sites (Cornell and Schwertmann 2003). The antiparallel Fe^{3+} spins on the A and B sites cancel out their magnetic contributions, and the net ferrimagnetism is caused by the Fe^{2+}, or another divalent cation, in the B sub-lattice, provided that this cation has unpaired electrons.

XMCD, which measures the difference between the core-level X-ray absorption spectra (XAS) using left and right circularly polarized X-rays in the vicinity of an absorption edge, is rich in information about the electronic and the magnetic structure of solid materials (van der Laan et al. 1986a; van der Laan and Thole 1991; Chen et al. 1995; Stöhr 1995; Schütz et al. 1997). Using synchrotron radiation, the absorption spectra of magnetic materials are collected in magnetic fields set parallel and antiparallel to the helicity vector of the X-rays, which is along the beam direction. Figure 2 shows the Fe $L_{2,3}$ absorption spectra of natural magnetite collected by reversing the applied 0.6 Tesla magnetic field; the difference between the two absorption spectra provides the XMCD spectrum (see Pattrick et al. 2002 for details). The application of 0.6 Tesla is not expected to magneti-

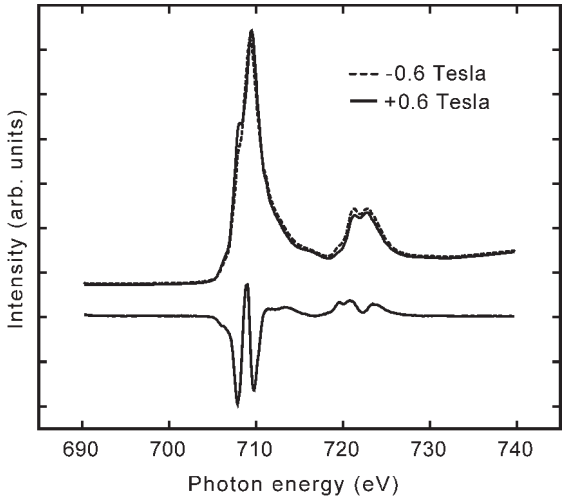

FIGURE 2. Fe $L_{2,3}$ absorption spectra of natural magnetite. The *L*-edge spectra were collected in a reversible 0.6 Tesla magnetic field, and the resulting XMCD difference spectrum is shown below (intensity scale enhanced by a factor of three).

cally saturate the sample. Although the strength of the applied field changes the shape of the spectra measured with positive and negative magnetization, it does not change the shape of the XMCD, only its magnitude. Note that peaks in the XMCD pointing up are denoted "positive" and those pointing down are "negative." Thus, Figure 2 shows three XMCD peaks around 710 eV (L_3-edge)—two large negative peaks with a positive peak in between.

XMCD is element-selective as it involves analysis of the $L_{2,3}$ edge absorption, which occurs at a specific photon energy for each element. The XMCD technique provides information about the oxidation state (including mixed states), site symmetry, spin state, and crystal-field splitting of the absorbing 3*d* transition metal ions. XMCD is also sensitive to the direction and size of the local magnetic moments. The orbital and spin contributions to the total magnetic moment can be separated through a theoretical analysis of the XMCD spectrum (van der Laan and Thole 1991; Stöhr 1995). Furthermore, the *sum rule*, developed by Thole (1992), states that the XMCD signal integrated over the 2*p* absorption edge is proportional to the orbital part of the 3*d* magnetic moment.

The $L_{2,3}$ absorption spectra for different polarization directions can be calculated using the method described by van der Laan and Thole (1991); calculation details are provided in Pattrick et al. (2002). The Fe $L_{2,3}$-edge XMCD spectrum for ferrite spinels could potentially show features for four different chemical environments, namely for Fe^{3+} and Fe^{2+} in each of the crystallographically distinct tetrahedral and octahedral sites. Brice-Profeta (2004) has shown that a 75:25 ulvöspinel:magnetite solid solution (i.e., titanomagnetite of stoichiometry $Fe^{2+}_{1.75}Fe^{3+}_{0.5}Ti^{4+}_{0.75}O_4$) has all four peaks: Fe^{2+} tetrahedral (positive peak at ~709.5 eV), Fe^{2+} octahedral (negative peak, ~710.5 eV), Fe^{3+} tetrahedral (positive peak, ~711.5 eV), and Fe^{3+} octahedral (negative peak, ~712.5 eV). The experimental XMCD spectrum for magnetite (Fig. 2) comprises only three main peaks resulting from Fe^{2+} octahedral (d^6O_h), Fe^{3+} tetrahedral (d^5T_d), and Fe^{3+} octahedral (d^5O_h) components; as expected no peak for tetrahedral Fe^{2+} is present. The Fe^{2+} occupancy of the tetrahedral site in magnetites and Ti-poor titanomagnetites is unlikely to be significant and is not considered further here.

The calculated spectra for the three main components in magnetites, along with the overall Fe_3O_4 spectrum taken as the sum of these components, are shown in Figure 3. Mixtures of these three theoretical components can, therefore, be fitted to experimentally derived spectra to produce occupancy ratios for the proportions of Fe^{2+} and Fe^{3+} in the octahedral site, and of Fe^{3+} in the tetrahedral site.

The thermodynamic, magnetic, and electrical properties of natural ferrite spinels are dependent on the type, concentration and distribution of cations within the spinel structure. Thus, the XMCD spectrum for stoichiometric magnetite (Fe_3O_4) will be significantly different to that of non-stoichiometric, "oxidized" magnetite ($Fe_{3-\delta}O_4$, where δ quantifies the deviation from stoichiometry due to cation vacancies). Note that the fully oxidized end-member is maghemite (γ-Fe_2O_3), which has the spinel formula $Fe^{3+}_{2.666}\square_{0.333}O_4$, where $\square$ represents a vacancy. The XMCD technique can provide direct information on the value for δ, as well as for the relative proportions of tetrahedral Fe^{3+}, octahedral Fe^{2+}, and octahedral Fe^{3+} (Schedin et al. 2004). The incorporation of other cations with ionic radii in the range 0.5 to 0.9 Å, such as Al, Mg, Mn, Ti, V, and Zn in the octahedral and tetrahedral sites, also has a profound effect on the XMCD spectrum of natural ferrite spinels.

Several XMCD studies have been carried out on synthetic stoichiometric and non-stoichiometric magnetites (Table 1). These studies, involving non-bulk materials such as thin films, nano-particles, and multilayers, draw attention to the versatility and value of the XMCD technique. However, a systematic XMCD study of natural bulk ferrite spinels has not previously been carried out. In this paper, the value of this technique for determining site occupancies, cation distribution, and the effects of non-stoichiometry in these materials is demonstrated.

EXPERIMENTAL METHODS

Twenty natural magnetite samples were studied using electron probe microanalysis (EPMA), X-ray diffraction, and XMCD. Many of these samples have similar compositions and XMCD spectra, therefore representative samples with compositions close to that of Fe_3O_4, along with samples containing high concentrations of other cations (Mg, Ti, Mn, and Zn), were selected for detailed examination in this paper. The morphological properties and provenance of these 10 samples are summarized in Table 2.

Chemical compositions were determined using wavelength-dispersiveEPMA employing a Cameca SX100 microprobe in the Williamson Research Centre at the University of Manchester. An operating voltage of 15 kV and a specimen current of 20 nA were used. Standardization was performed using a combination of simple oxides, silicates, and pure metal standards. Counting times of 50 s for peak measurement and 50 s for background measurement were employed; all matrix corrections were carried out using the Cameca PAP correction routine. To characterize sample homogeneity, five to ten analyses were performed for 11 different elements (Co, Ni, Zn, Fe, Mn, Ti, V, Cr, Si, Al, and Mg) on each of the magnetite samples. Analyses of major elements were accurate to within 1% (relative) of the amount present and to within 5% for minor elements.

X-ray diffraction patterns of the powdered magnetite samples were obtained using Cu$K\alpha$ radiation with a Philips PW1060 X-ray diffractometer equipped with a curved-crystal graphite monochromator. The cell parameters were determined from the data using the UNITCELL program (Holland and Redfern 1997) with Si employed as an internal standard.

TABLE 1. Summary of selected studies of synthetic stoichiometric magnetite, nonstoichiometric magnetite, end-member spinel ferrites, and mixed-cation spinel ferrites reported in the literature

Spinel ferrites studied	Techniques used	Comments	Author and Year
Fe_3O_4	XMCD	Probably, the first reported Fe $L_{2,3}$ XMCD of Fe_3O_4.	(Sette et al. 1990)
Fe_3O_4	X-ray linear and circular magnetic dichroism	Linear dichroism in Fe_3O_4 larger but more difficult to measure than circular dichroism. Best fit for absorption multiplets of Fe $d^5$and Fe d^6 ions in A and B sites for all polarization directions calculated. The spectra of Fe_3O_4 could be used as a fingerprint for these oxides.	(Kuiper et al. 1997)
Fe_3O_4 $Fe_{3-\delta}O_4$ γ-Fe_2O_3	XMCD	XMCD spectra obtained for a range of intermediated phases from magnetite (Fe_3O_4, $\delta = 0$) to maghemite (γ-Fe_2O_3, $\delta = 1/3$). Nanocrystalline Fe_2O_3 anlyzed using XMCD.	(Pellegrin et al. 1999)
$NiFe_2O_4$	XMCD	Application of XMCD to ferromagnetic oxides. Orbital polarization in $NiFe_2O_4$ measured by Ni $L_{2,3}$ XMCD.	(van der Laan et al. 1999)
Fe_3O_4	XMCD, conversion electron Mössbauer spectroscopy (CEMS)	XMCD and CEMS of ultrathin epitaxial Fe_3O_4 films on Pt(111). Relative occupancy of tetrahedral and octahedral sites derived from CEMS and XMCD data different due to differences in film thickness.	(Schedin et al. 2000)
Fe_3O_4	XMCD	Comparison of XMCD in samples of colloidal Fe_3O_4 and in Fe_3O_4 powder. Dichroism spectra of colloidal (particle size = ~1 μm) and bulk Fe_3O_4 qualitatively the same but with a shift in the position of the Fe L_3 line in the colloid with regard to the powder.	(de Castro et al. 2001)
$(Co,Zn)FeO_4$	XMCD	Cation distribution in mixed cobalt-zinc ferrite nanoparticles evaluated. Preference of Co^{2+} for O_h sites and Zn^{2+} for T_d sites verified.	(Hochepied et al. 2001)
Fe_3O_4 $MgFe_2O_4$ $NiFe_2O_4$ $CoFe_2O_4$ $ZnFe_2O_4$ Mixed spinel ferrites	XMCD	XMCD used to study cation site occupancies in a series of synthetic spinel ferrites and in natural magnetite. XMCD spectra varied significantly with spinel composition. Differences quantified by fitting three components of calculated spectrum. Calculated fit of bulk natural magnetite did not produce 1:1:1 ratio of site occupancy.	(Pattrick et al. 2002)
$Fe_{3-\delta}O_4$	XMCD, CEMS	Thin films of Fe_3O_4 and $Fe_{3-\delta}O_4$ grown epitaxially on Pt^{3+} were analyzed. Information about orientation of magnetic moments and individual close packed/loose packed octahedral site ratios obtained from CEMS. Concentration of Fe^{3+}_{Td}, Fe^{2+}_{Oh}, and Fe^{3+}_{Oh} relative to stoichiometric Fe_3O_4 obtained from XMCD allowed A:B ratio to be determined and δ to be determined for $Fe_{3-\delta}O_4$.	(Morrall et al. 2003)
Fe_3O_4	XMCD	XMCD measurements analyzed using calculations based on full-multiplet cluster model to extract electronic structure parameters of Fe_3O_4 containing different spin and oxidation states. Results indicate that Fe_3O_4 is a system with strong electron-electron interactions.	(Chen et al. 2004)
Fe_3O_4	XMCD, superconducting quantum interference device (SQUID) magnetometer	Single crystals of Fe_3O_4 measured using XMCD and SQUID to determine spin and orbital magnetic moments. Underlying physics of magnetic moments of Fe_3O_4 unraveled using cluster-model calculations and band-structure calculations.	(Huang et al. 2004)
Fe_3O_4 $Fe_{3-\delta}O_4$	XMCD	Information about stoichiometries, δ in $Fe_{3-\delta}O_4$ and relative site occupancies of Fe^{3+}_{Td}, Fe^{2+}_{Oh}, and Fe^{3+}_{Oh} ions obtained by comparing XMCD data to calculated dichroism spectra.	(Schedin et al. 2004)
Fe_3O_4	XMCD, magneto-optical Kerr effect (MOKE) and photoemission	Thin films of Fe_3O_4 on GaAs(100) show uniaxial magnetic anisotropy in thickness range 2–6 nm.	(Lu et al. 2004)
Fe_3O_4 γ-Fe_2O_3 $ZnFe_2O_4$ $Fe_{2-x}Ti_xO_4$	XMCD	Study of structural and magnetic properties of nano-sized spinel oxide systems: preferential surface spin disorder of Fe^{3+}_{Oh} ions in δ-Fe_2O_3; magnetic disorder in $ZnFe_2O_4$ increases as magnetic dilution with Zn^{2+}_{Td} increases; Ti^{4+} involved in magnetic exchange couplings in $Fe_{2-x}Ti_xO_4$.	(Brice-Profeta 2004)

TABLE 2. Natural magnetite samples examined in detail in this study

Sample locality	Sample description	Geological context
Dekoa, Bangui, Central African Republic	Euhedral Octahedra in meta-basic schist	Highly metamorphosed (2.5 Ga) Archeaen Greeenstone Belt. Subsequent retrograde metamorphism.
ZCA Number 4 Mine, Balmat, New York, U.S.A.	Euhedral cubic, with matrix of anhydrite and calcite.	Associated with low temperature base-metal mineralization in late-Precambrian marbles – metamorphosed to 6.5 kbar/625 °C during Grenvillian (1 Ga) (Steers 2003).
Marmora Iron Mine, Madoc Area Canada	Massive/acicular form associated with Fe-sulfides	Massive skarn in Ordovician marbles, overlying Grenvillian.
Erzgebirge, Germany	Massive	Carbonate-hosted skarn assoc. late Palaeozoic granites.
Iron Mountain, Utah, U.S.A. (M855)	Octahedral euhedral	Replacement of Jurassic limestone by fluids assoc. with Miocene quartz-monzonite laccolith (Barker 1995).
Bushveld SA 620, South Africa	Massive granular assoc. Fe-Ti-oxides	Gabbro-hosted Ti-rich magnetite layer in Upper Zone of ca 2.0 Ga Bushveld Intrusion, formed during magma mixing during crystallization (Harney and von Gruenewaldt 1995).
Bushveld SA 637, South Africa	Massive granular assoc. Fe-Ti-oxides	As above.
Marangudzi T203, Zimbabwe	Subhedral grains in gabbro	Gabbro sheet intruded by ring dykes of quartz syenite and cone sheets of nepheline syenite (Hossain and Henderson 1977), Nuanetsi Igneous Province, Zimbabwe (Cox et al. 1965).
Långban, Sweden	Sub-octahedral and cubiform	Late Archaean carbonate-hosted skarn-like Fe+Mn oxide ore bodies of probable exhalative origin and affected by extensive high-grade metamorphism and multiphase granite intrusion.
Franklin, New Jersey, U.S.A.	Massive granular	Massive lens of magnetite associated with metal-rich, mid-Proterozoic submarine exhalative fluids, subsequently metamorphosed during late Grenvillian orogeny.

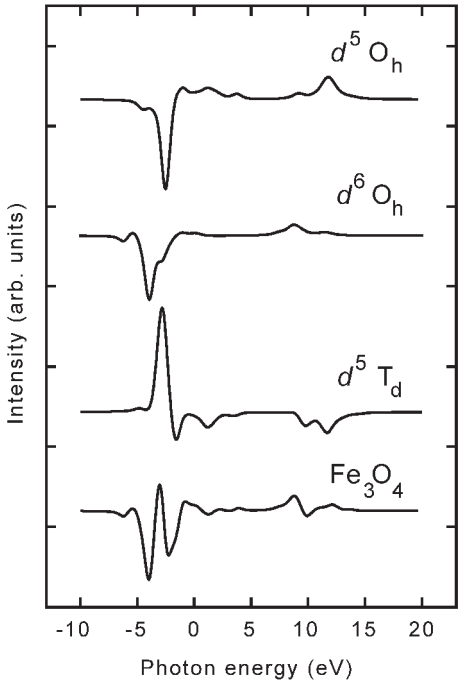

FIGURE 3. The calculated Fe d^6O_h, Fe d^5T_d, Fe d^5O_h components of the XMCD spectrum and the resulting summed calculated spectrum of Fe_3O_4 (adapted from Pattrick et al. 2000)

XMCD of the samples were measured using the 0.6 Tesla magnet sample chamber (the "Flipper") on beamline 1.1 of the Synchrotron Radiation Source (SRS) at Daresbury Laboratory (Dudzik et al. 2000). This beamline is equipped with a high-energy spherical grating monochromator, which was set to provide 75% circularly polarized X-rays in the energy region of interest. The energy was calibrated by measuring the Fe L_3 peak of Fe metal and the Marmora magnetite, assuming a photon energy of 707.7 eV for pure Fe metal (Chen et al. 1995). The magnetite samples were ground to a powder, using a pestle and mortar, immediately prior to measurement to minimize any surface oxidation. Slices of the Bangui magnetite were also cut with (100) and (111) orientations. The finely powdered samples and the slices were mounted onto the copper plate of the sample manipulator using strips of conducting carbon tape. The sample manipulator was placed in a vacuum chamber (10^{-7} mbar) between the coils of an electromagnet with soft-iron pole pieces. Magnetic fields were generated up to ±0.6 Tesla with a polarity switching time of 0.5 s. The direction of the applied magnetic field was aligned along the light helicity vector, with the sample normal aligned at an angle of 45° to the beam. The XMCD data were corrected for the saturation as well as for the degree of circular polarization.

The total-electron-yield X-ray absorption signal was recorded in drain current mode and normalized to the incident X-ray flux. The electron-escape depth is expected to be ~50 Å and the photon absorption length equal to 254 and 653 Å at the L_3 and L_2 edges, respectively (Huang et al. 2004). Therefore the condition that the drain current is linear with the X-ray absorption signal is reasonable well fulfilled (van der Laan and Thole 1988), while the probing depth is large enough to measure a representative part of the sample. The XAS data were collected over three regions: a 25 eV pre-edge region with an energy step size of 0.5 eV, an edge region (700–735 for Fe, 635–670 for Mn, and 450–485 eV for Ti) with an energy step size of 0.2 eV and a 10 eV post-edge region with an energy step size of 0.5 eV. The counting time was maintained at 1 s per energy point. The XMCD spectra were obtained by flipping the magnetization direction for each photon energy and taking the difference of these two absorption measurements. All data were recorded at room temperature, and the measured spectra were reproducible in repeated scans.

The areas for the three main peaks (i.e., those due to Fe d^6O_h, Fe d^5T_d, and Fe d^5O_h components) were fitted over the energy range 704–712 eV using the program CFIT developed at Daresbury Laboratory (Kirkman, pers. comm.). To assess the reliability of the fits, a magnetite sample was measured and analyzed four separate times to give mean values for the three main peaks of Fe d^6O_h: 1.05 ± 0.03, Fe d^5T_d: 0.96 ± 0.02, and Fe d^5O_h: 0.99 ± 0.04. These values give a Fe^{2+}/Fe^{3+} ratio, with propagated 1σ errors, of 0.54 ± 0.04.

The *L*-edge XAS for the non-Fe transition metal cations Ti and Mn were recorded (also on beamline 1.1 of the SRS) for the natural ferrite spinel samples that contained large enough concentrations of these elements. The sample prepara-

TABLE 3. Elemental composition of natural ferrite spinels derived using EPMA (wt% deficiency can be assigned to oxygen), along with cell parameters derived using XRD

	wt%												
Sample	Co	Ni	Si	Ti	Al	Mg	V	Cr	Mn	Zn	Fe	Total	Cell parameter *a* (Å), (1σ)
Bangui	0.00	0.01	0.00	0.01	0.02	0.03	0.03	0.00	0.05	0.00	72.51	72.65	8.3923 (12)
ZCA	0.00	0.00	0.05	0.01	0.00	0.01	0.01	0.00	0.01	0.92	71.43	72.44	8.3985 (5)
Marmora	0.00	0.00	0.20	0.00	0.00	0.20	0.00	0.00	0.18	0.01	71.95	72.55	8.3980 (8)
Erzgebirge	0.00	0.01	0.08	0.03	0.47	0.13	0.00	0.00	0.49	0.09	70.89	72.12	8.3927 (10)
Iron Mountain	0.00	0.03	0.00	0.24	0.07	0.48	0.09	0.00	0.08	0.03	70.76	71.79	8.3936 (7)
Bushveld SA 620	0.00	0.01	0.01	9.14	1.55	0.97	0.39	0.07	0.21	0.03	56.65	69.04	8.3659 (5)
Bushveld SA 637	0.00	0.05	0.02	8.34	1.52	0.98	0.93	0.15	0.19	0.04	55.65	67.88	8.3543 (8)
Marangudzi T 203	0.00	0.05	0.01	3.07	1.41	0.16	0.43	0.15	0.22	0.11	65.63	71.23	8.3941 (5)
Långban	0.00	0.00	0.00	0.00	0.32	9.36	0.00	0.00	4.02	0.50	54.93	69.14	8.4673 (13)
Magnesio-ferrite (syn)	0.00	0.01	0.00	0.00	0.00	11.19	0.00	0.00	0.12	0.01	56.34	67.69	8.3887 (4)
Franklin	0.00	0.01	0.00	0.01	0.37	0.24	0.01	0.00	7.48	12.31	51.57	72.00	8.4578 (12)
Zinc ferrite (syn)	0.01	0.02	0.01	0.00	0.00	0.04	0.00	0.00	0.11	17.79	53.85	71.82	8.4242 (6)

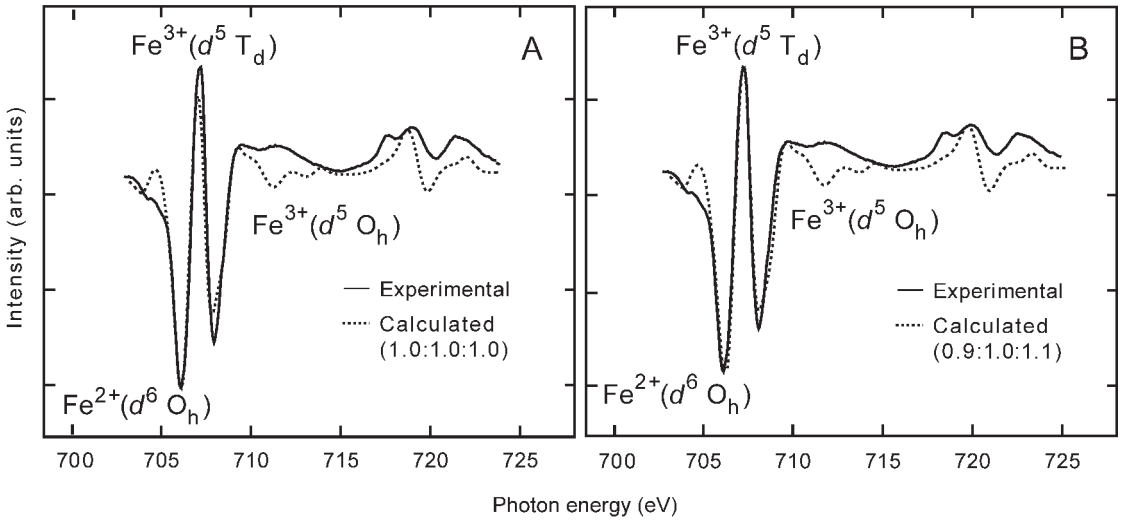

FIGURE 4. Comparison of the experimentally derived standard natural magnetite (Bangui) XMCD spectrum (solid line) and the calculated XMCD spectrum (dashed line) for (**a**) Fe_3O_4 and (**b**) $Fe_{3-\delta}O_4$.

tion and measurement conditions were as described above, without the application of the magnetic field. Ti measurements were made without the application of the magnetic field.

RESULTS

Microprobe analyses and unit-cell parameters

Microprobe analyses are reported in Table 3 as element wt%, so that no assumption is made regarding the Fe^{2+}:Fe^{3+} ratio at this stage; most of the samples studied contain only minor amounts of other elements (less than 1%). However, the Bushveld and Marangudzi samples are Ti-bearing with significant amounts of Al^{3+} and V^{3+}, the Långban sample has a significant magnesio-ferrite component, and the Franklin sample is characteristically rich in Zn^{2+} and Mn^{2+}/Mn^{3+}. The presence of the major amounts of smaller Ti^{4+} ions in the Bushveld samples and of larger Mn^{2+}/Mn^{3+} and Zn^{2+} ions in the Franklin sample is reflected in their smaller and larger unit-cell parameters, respectively (Shannon 1976), compared to values for samples closer to end-member stoichiometric magnetite, as shown in Table 3. Cell parameters given here are generally in agreement with those of Waychunas (1991) for similar compounds.

XMCD analysis of "standard" natural magnetite from Bangui

Several XMCD analyses of the sample from Bangui (Fig. 4) were obtained to examine the effect of crystallographic orientation as well as the effect of using a powder or bulk sample. The differences found were minimal. This sample is very low in trace elements (near end-member magnetite, Fe_3O_4) and is therefore used as a "standard" in this study. XMCD analysis of the other natural magnetites that contained very low concentrations of impurity elements produced spectra similar to that obtained for the Bangui sample.

The average Bangui (powder and bulk) spectrum is compared to the calculated spectrum of stoichiometric magnetite (Fe_3O_4), calculated from the sum of the d^6O_h, d^5T_d, and d^5O_h components, in Figure 4a. It can be seen that most of the disagreement between the calculated and experimental spectra occurs at photon energies above the L_3 edge (>711 eV). This is because above the L_3 edge, the theoretical calculation shows a low-intensity multiplet structure, which is broadened in the experimental spectra, indicating the presence of charge-transfer satellites. Strictly speaking, several electronic configurations that are hybridized with each other should be taken into account; this introduces several extra

parameters, including the charge-transfer energy (i.e., the energy difference between the different configurations) and the hybridization strengths. However, the charge-transfer satellites in XAS are small due to the efficient screening of the core electron that is excited directly into the 3*d* shell (van der Laan et al. 1986b). Therefore, no significant improvement is achieved by taking the extra configurations into account; indeed the calculated spectra of Chen et al. (2004), which include these configurations, show little improvement over those that use a single configuration (Kuiper et al. 1997; Pattrick et al. 2002; Morrall et al. 2003; Schedin et al. 2004). Moreover, the peak intensity is a direct measure of the magnetic moment, and most intensity is in the leading peaks (cf. Fig. 3). Therefore, the fitting procedure used here is concentrated mainly on the three peaks of interest in the L_3 region at 706, 708, and 710 eV (Fig. 4); the fact that the middle peak has the opposite sign to those of the two outer peaks is an enormous advantage in the curve fitting process.

It can also be seen that the small positive peak at the onset of L_3 (707 eV) in the calculated spectrum is not resolved in the experimentally derived spectrum. This problem was also noted by Kuiper et al. (1997) and Pattrick et al. (2002), and it was suggested that it could be solved by including the low-lying thermally excited states of Fe d^6 in the calculation. A small negative feature can be seen in the experimental XMCD spectrum at 707 eV (Fig. 4), which seems to be related to the d^6 contribution. This feature is not visible in the XMCD spectra for those ferrite spinels containing high concentrations of cations such as Zn replacing Fe in the d^6O_h site. However, as the calculated spectrum does not match the experimentally derived spectrum in this region, it is difficult to attach significance to this feature.

Figure 4 shows that the experimental spectrum for natural magnetite does not exactly match the three peaks of interest in the calculated spectrum of stoichiometric magnetite. The d^6O_h and d^5T_d features are reproduced reasonably well in the experimental spectrum, the main difference being the higher intensity of the calculated Fe d^5O_h peak (Fig. 4a). In fact, the spectrum more closely resembles the XMCD spectra reported for non-stoichiometric, nanocrystalline magnetite, and magnetite ultra-thin films ($Fe_{3-\delta}O_4$) with a stoichiometry between that of magnetite (Fe_3O_4, $\delta = 0$) and maghemite (γ-Fe_2O_3, $\delta = 1/3$) (Fig. 4b) (Pellegrin et al. 1999; Morrall et al. 2003; Schedin et al. 2004). The similarity between the spectra obtained in these literature studies and the spectra obtained for 13 of the natural samples analyzed suggest that most natural ferrite spinels deviate from stoichiometric magnetite and contain vacancies in their structure. This issue is discussed further below.

Fe site occupancy and spinel non-stoichiometry

The apparent Fe site-occupancy ratios have been calculated from experimentally derived XMCD spectra peak areas by comparison with the theoretically derived components Fe d^6O_h, Fe d^5T_d, and Fe d^5O_h (see Fig. 3). The Fe^{2+} and Fe^{3+} values derived from the XMCD site occupancies were then used in combination with the analytical data obtained from EPMA (Table 3) to determine the spinel compositions and stoichiometries of the ferrite spinels (Table 4). At this stage the analyses are converted to oxide components with cation numbers normalized to 4 O atoms per formula unit. The cation totals shown in Table 4 for some samples are smaller than 3.0, the value assumed for stoichiometric spinel, pointing to the presence of cation vacancies. By varying different parameters, it was determined that the errors associated with the EPMA data and the fitted XMCD data resulted in an absolute error in the vacancies of ±0.01.

The conventional approach in dealing with electron microprobe analyses of spinels is to report the elements as oxides with all Fe as FeO, which gives low analytical totals and high cation numbers (>3.0) for a 4 O atom formula unit. Droop (1984) has used a simple general equation to determine the Fe^{2+}/Fe^{3+} ratio for stoichiometric minerals as follows:

$$F = 2X\,(1 - T/S),$$

where F is the number of Fe^{3+} ions present per X O atoms, T is the correct cation total, and S is the observed cation total. However, in the case of minerals with cation vacancies, such as nonstoichiometric spinels in which the formula unit deviates from 3 cations for 4 O atoms, this equation is not rigorous and must be applied with caution. It can be seen in Table 4 that many of the natural ferrite spinels studied here are non-stoichiometric and contain cation vacancies, which suggests that the Fe^{2+}/Fe^{3+} calculated from the XMCD will differ from those determined using Droop's formula; the actual results are compared in Table 5. The XMCD Fe^{2+}/Fe^{3+} ratio (0.61 ± 0.04) was also compared with that determined by chemical analysis (0.55 ± 0.03) for the titanomagnetite sample (T 203) from Marangudzi and the agreement is within a 1σ error.

For the ferrite spinels without vacancies (Erzgebirge and Iron

TABLE 4. Spinel compositions, Fe site occupancies, and cation vacancies for spinel ferrites calculated from EPMA data and XMCD difference spectra

Sample	Spinel cation composition	d^6O_h	d^5T_d	d^5O_h	Cation total	Vacancy
Bangui	$Fe_{2.96}$	0.88	1.00	1.08	2.96	0.04
Marmora	$Mg_{0.02}Mn_{0.01}Si_{0.02}Fe_{2.92}$	0.89	0.96	1.07	2.97	0.03
ZCA	$Zn_{0.03}Fe_{2.95}$	0.93	0.97	1.05	2.98	0.02
Erzgebirge	$Al_{0.04}Mg_{0.01}Mn_{0.02}Si_{0.01}Fe_{2.92}$	0.98	1.01	0.93	3.00	0.00
Iron Mount.	$Al_{0.01}Mg_{0.05}Ti_{0.01}Fe_{2.93}$	0.96	0.90	1.07	3.00	0.00
Bushveld SA 637	$Al_{0.12}Cr_{0.01}Mg_{0.08}Mn_{0.01}Ti_{0.37}V_{0.04}Fe_{2.10}$	0.41	0.75	0.94	2.73	0.27
Bushveld SA 620	$Al_{0.12}Mg_{0.08}Mn_{0.01}Ti_{0.39}V_{0.02}Fe_{2.08}$	0.40	0.73	0.95	2.70	0.30
Marangudzi T203	$Al_{0.12}Cr_{0.01}Mg_{0.02}Mn_{0.01}Ti_{0.14}V_{0.02}Fe_{2.64}$	1.00	0.87	0.77	2.96	0.04
Långban	$Al_{0.03}Mg_{0.80}Mn_{0.15}Zn_{0.02}Fe_{2.05}$	0.19	0.75	1.11	3.05	–0.05
Magnesio-ferrite (syn)	$Mg_{0.95}Mn_{0.01}Fe_{2.09}$	0.19	0.90	1.00	3.05	–0.05
Franklin	$Al_{0.03}Mg_{0.02}Mn_{0.33}Zn_{0.45}Fe_{2.21}$	0.39	0.62	1.20	3.04	–0.04
Zinc ferrite (syn)	$Mn_{0.01}Zn_{0.67}Fe_{2.36}$	0.45	0.61	1.30	3.04	–0.04

Note: The spectra were fitted for three main spectral features derived from the Fe L_3 peaks only and ratios calculated to the number of Fe atoms per unit spinel formula on a 4 O basis.

TABLE 5. Fe^{2+}/Fe^{3+} ratios obtained using XMCD site occupancies and EPMA data, in relation to any vacancies present in the structures

Locality of magnetite	Fe^{2+}/Fe^{3+} ratios from EPMA data (Droop 1984)	Fe^{2+}/Fe^{3+} ratios from EPMA + XMCD data	Vacancies
Bangui Region, C.A.R.	0.50	0.42	0.04
Marmora, Canada	0.50	0.44	0.03
ZCA mine, U.S.A.	0.49	0.46	0.02
Erzgebirge, Germany	0.50	0.50	0.00
Iron Mountain, U.S.A.	0.49	0.49	0.00
Bushveld SA 637, S.A.	1.30	0.25	0.27
Bushveld SA 620, S.A.	1.37	0.24	0.30
Marangudzi T203, Zimbabwe	0.72	0.61*	0.04
Långban, Sweden	0.02	0.11	–0.05
Magnesio-ferrite (syn)	0.03	0.10	–0.05
Franklin, U.S.A.	0.11	0.21	–0.06
Zinc ferrite (syn)	0.17	0.24	–0.06

* A wet chemical analysis gives an Fe^{2+}/Fe^{3+} atomic ratio of 0.55±0.03 (Hossain 1970).

Mountain), the Fe^{2+}/Fe^{3+} ratios calculated using the two different methods are the same. However, a poor correlation is obtained for the Fe^{2+}/Fe^{3+} ratios calculated for non-stoichiometric spinels, with the difference between iron oxidation state ratios increasing with increasing cation vacancies. The difference between the ratios obtained by the two different methods for the Bushveld samples is particularly striking, but even small proportions of vacancies have a marked effect on the correlation.

DISCUSSION

Cation distribution in natural spinels depend on the original formation temperature and subsequent cooling history of the host rock (e.g., O'Neill et al. 1992), as well as the size and charge of the cation. Based on previous work (Carbonin et al. 1996; Lucchesi et al. 1999) the assumed distribution for the non-Fe cations in natural ferrite spinels is shown in Table 6. The Fe^{2+}/Fe^{3+} cation distribution, shown in Table 4, has been used along with the data in Table 6 to analyze site occupancy in the natural ferrite spinels.

CATION-DEFICIENT FERRITE SPINELS

The vacancy concentrations (Table 5) in ferrite spinels from Bangui, Marmora, and ZCA suggest that they are cation-deficient oxidized ferrite spinels ($Fe_{3-\delta}O_4$), which have a stoichiometry between those of magnetite (Fe_3O_4) and maghemite (γ-Fe_2O_3). Since charge neutrality has to be maintained, these minerals can be represented by the formula

$$Fe^{3+}_{A}\,[Fe^{2+}_{1-3\delta}\,Fe^{3+}_{1+2\delta}\,\square_{\delta}]_{B}\,O_4. \quad (1)$$

In maghemite, the vacancies have a strong preference for B sites (Gillot 1994). δ must lie in the range 0 to 1/3 corresponding to magnetite and maghemite, respectively (Schedin et al. 2004). The Bangui, Marmora, and ZCA samples with δ values in the range 0.01 to 0.04 are, thus, very close to the magnetite-end of this series.

The XMCD spectra obtained from these cation-deficient magnetite-maghemites are shown in Figure 5; 13 of the 15 analyzed samples with compositions close to end-member magnetite have XMCD spectra similar to those shown in this figure.

The fit for the experimentally derived Fe XMCD spectrum for the Bangui magnetite ($Fe_{2.96}\square_{0.04}O_4$) indicates a ratio of 0.88 Fe d^6O_h, 1.00 Fe d^5T_d, 1.08 Fe d^5O_h (Table 4). This sample does not contain significant amounts of any other cations and the total occupations for the single tetrahedral and two octahedral sites can therefore be given as n(A) = 1.00, n(B) = 1.96 (where A and B refer to T_d and O_h sites). Thus, employing Equation 1 for cation-deficient magnetites, the ratio is $1–3\delta:1:1+2\delta$, where $\delta = 0.04$. Significantly this value of δ was also obtained for a non-stoichiometric ultrathin $Fe_{3-\delta}O_4$ (111) film, grown epitaxially on Al_2O_3 (0001), and characterized using XMCD (Schedin et al. 2004). Bangui magnetite can therefore be taken as an example of a typical natural (unsubstituted) $Fe_{3-\delta}O_4$ magnetite.

The fit for the Marmora spinel ($Mg_{0.02}Mn_{0.01}Si_{0.02}Fe_{2.92}\square_{0.03}O_4$)

TABLE 6. Typical cation distribution of trace elements in spinel ferrites

Cation	Tetrahedral (A) Site (%)	Octahedral (B) Site (%)
Al^{3+}	0–10	90–100
Cr^{3+}	0	100
Mg^{2+}	10–30	70–90
$Mn^{2+/3+}$	85–100	0–15
Si^{4+}	100	0
Ti^{4+}	0	100
V^{3+}	100	0
Zn^{2+}	25–100	0–75

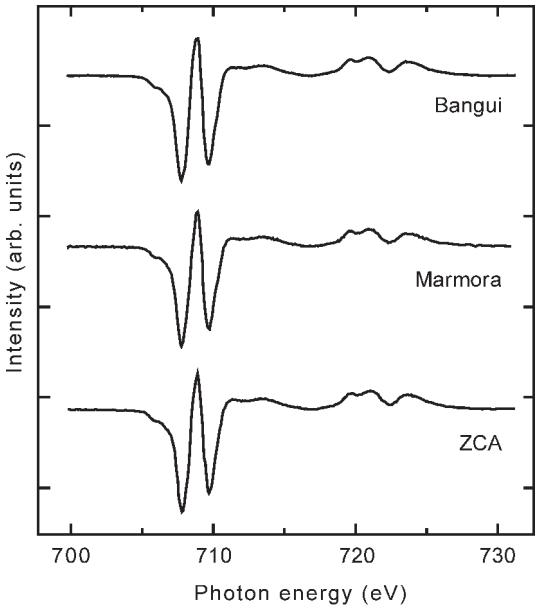

FIGURE 5. The experimentally derived XMCD spectra of natural cation-deficient ferrites from Bangui ($Fe_{2.96}O_4$), Marmora ($Mg_{0.02}Mn_{0.01}Si_{0.02}Fe_{2.92}O_4$), and ZCA ($Zn_{0.03}Fe_{2.95}$). Note the similar XMCD spectra.

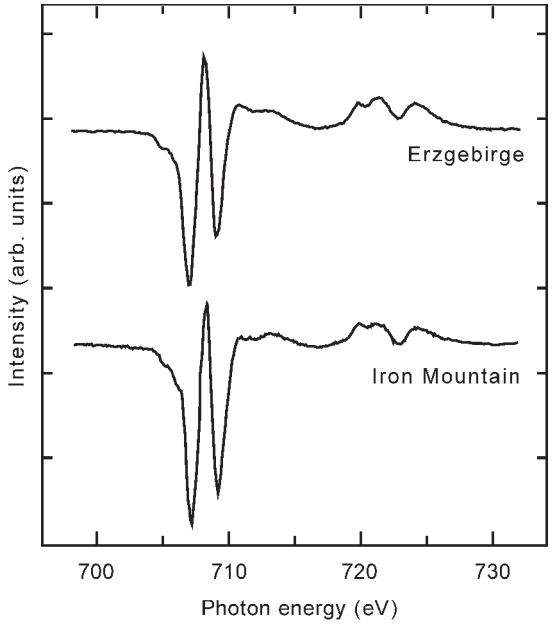

FIGURE 6. The experimentally derived XMCD spectra of natural stoichiometic ferrites from Erzgebirge ($Al_{0.04}Mg_{0.01}Mn_{0.02}Si_{0.01}Fe_{0.92}O_4$) and Iron Mountain ($Al_{0.01}Mg_{0.05}Ti_{0.01}Fe_{2.93}O_4$).

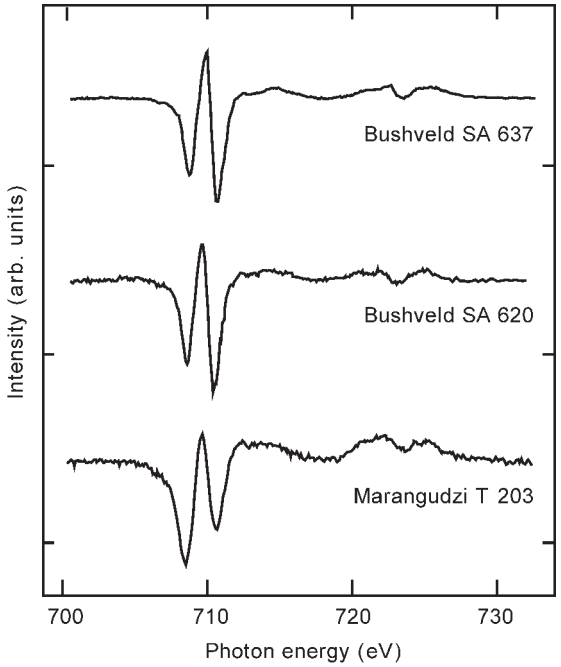

FIGURE 7. The experimentally derived XMCD spectra of natural titanium-rich ferrites from the Bushveld, SA 637 ($Al_{0.12}Cr_{0.01}Mg_{0.08}Mn_{0.01}Ti_{0.37}V_{0.02}Fe_{2.10}O_4$) and SA 620 ($Al_{0.12}Mg_{0.08}Mn_{0.01}Ti_{0.39}V_{0.02}Fe_{2.08}O_4$), and from Marangudzi T 203 ($Al_{0.12}Cr_{0.01}Mg_{0.02}Mn_{0.01}Ti_{0.14}V_{0.02}Fe_{2.64}O_4$)—intensity scale enhanced by a factor of 2.5 for SA 620 and T 203.

XMCD spectrum taken together with the minor element contents provides site occupancies of n(A) = 1.00, n(B) = 1.97, and the fit for the ZCA spinel ($Zn_{0.03}Fe_{2.95}\square_{0.02}O_4$) indicates n(A) = 1.00, n(B) = 1.98, if the cation distribution in Table 6 is employed. Note that the tetrahedral site is fully occupied for these three samples [n(A) = 1.00] indicating that the vacancies occur only in the octahedral sites as has been widely claimed for ferrite spinels (e.g., Gillot 1994).

Stoichiometric ferrite spinels

Charge balance, with a stoichiometry of 3 cations to 4 O atoms per spinel formula unit, was found for only two of the 15 analyzed samples with compositions close to end-member magnetite (Erzgebirge and Iron Mountain). The XMCD spectra obtained from these stoichiometric magnetites are shown in Figure 6. Incorporating the non-Fe cations as listed in Table 6, the XMCD and EMPA data for the Erzgebirge magnetite ($Al_{0.04}Mg_{0.01}Mn_{0.02}Si_{0.01}Fe_{2.92}O_4$) indicate n(A) = 1.02, n(B) = 1.98, which is within error of the n(A):n(B) ratio of 1:2. However, n(A) = 0.93, n(B) = 2.07 is obtained for the Iron Mountain magnetite ($Al_{0.01}Mg_{0.05}Ti_{0.01}Fe_{2.93}O_4$), the low tetrahedral site occupancy of 0.93 suggesting a less-ordered structure than is expected for stoichiometric magnetite. The excess of Fe^{3+} in the B site presumably occurs as cation interstitials (Goss 1988). Our XMCD results show that the presence of Ti in titanomagnetites is accompanied by tetrahedral vacancies, and it is possible that such vacancies in the Iron Mountain sample might be related to its small Ti content.

Cation-deficient titanium-rich ferrite spinels

Two of the Ti-bearing spinels examined (SA 620 and SA 637) come from magnetite-dominated layers within the upper zone of the Bushveld intrusion. Both magnetite (Fe_3O_4)-ulvöspinel ($Fe_2^{2+}TiO_4$) and ilmenite ($FeTiO_3$)-hematite (Fe_2O_3) compositions occur in these layers, often as complex exsolution textures formed during late- and post-magmatic cooling and hydrothermal alteration processes. Oxidation of titanomagnetite to Ti-bearing maghemite (hereafter referred to as titanomaghemite) is also a characteristic feature. SA 637 comprises 95% titanomaghemite, with minor exsolved spinel, ilmenite, and feldspar while SA 620 is composed of 60% of remnant titanomaghemite cores surrounded by rims of magnetite-ilmenite breakdown products; a minor TiO_2 phase is also present. Compared to titanomaghemite, the very weakly magnetic ilmenite will not contribute significantly to the XMCD spectrum. This is highlighted by the similarity between the XMCD spectra for SA 620 and SA 637, although the intensity of the signal is weaker for SA 620 as it contains less magnetic material (Fig. 7). The spinel compositions for SA 620 and SA 627, calculated from EPMA data, are also quite similar (Table 4) as the selected probe points correspond to the titanomaghemite areas contributing to the XMCD spectra. The other Ti-bearing spinel (T 203) comes from a Marangudzi gabbro where it occurs as relatively homogeneous subhedral grains with less abundant grains of ilmenite. This sample shows much less post-magmatic alteration than the Bushveld samples.

The coordination environment of the Ti was obtained by examining the Ti L edge XAS spectra of the Ti-bearing samples. The experimental spectra are shown in Figure 8, together with calculated spectra for Ti in both octahedral (O_h symmetry with $10Dq$ = 2.0 eV) and tetrahedral sites (T_d symmetry with $10Dq$ = –1.0 eV) calculated using atomic multiplet theory (van der Laan

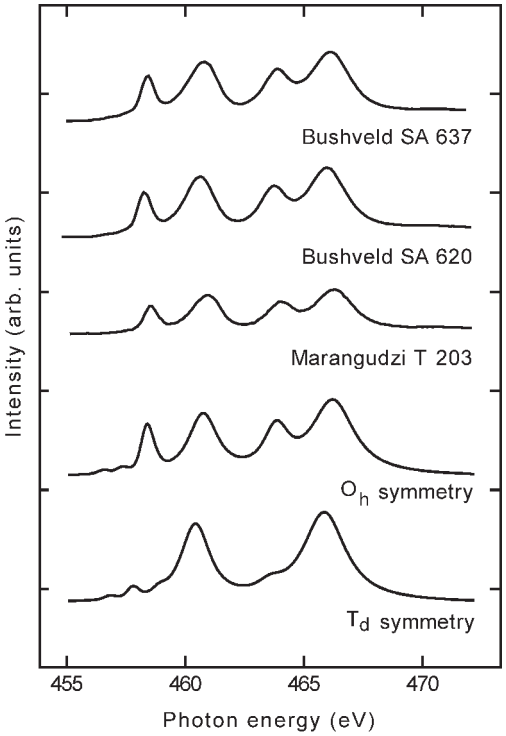

FIGURE 8. Ti $L_{2,3}$ XAS spectra. The experimental spectra for the Bushveld and Marangudzi titanomagnetites together with calculated spectra for O_h symmetry ($10Dq$ = 2.0 eV) and T_d symmetry ($10Dq$ = –1.0 eV).

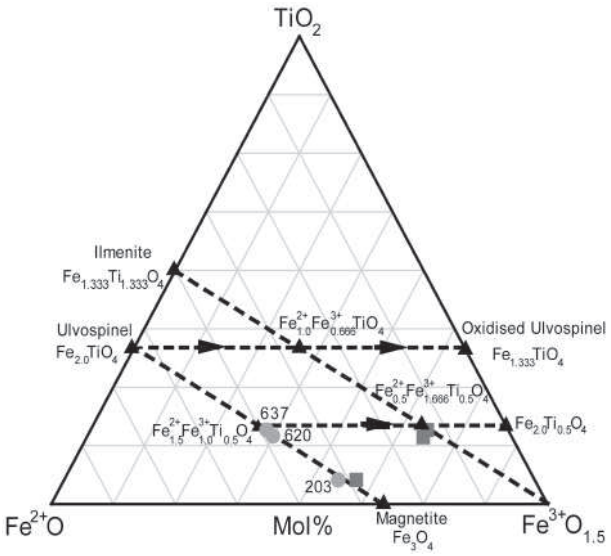

FIGURE 9. Phase composition in the system FeO-$FeO_{1.5}$-TiO_2 (mol%). The horizontal dashed lines with arrows mark the oxidation of ulvöspinel and of a 50:50 ulvöspinel-magnetite solid solution according to the reaction 1 $Fe^{2+} \rightarrow 0.666\ Fe^{2+} + 0.333\ \square$. The chemical formulae given are all on the basis of a spinel formula unit (4 O atoms). Ideal phase compositions (filled triangles); titanium-rich ferrite spinel compositions calculated from XMCD data for samples T 203, SA 637, and SA 620, this work (gray squares); titanium-rich ferrite spinel compositions calculated on a basis of 4 O atoms and 3 cations for samples T 203, SA 637, and SA 620 (Droop 1984) (gray circles).

and Thole 1991; van der Laan and Kirkman 1992). The XAS shows clearly that the Bushveld and Marangudzi samples contain Ti as $Ti^{4+}O_h$ (van der Laan 1990). The presence of ilmenite in SA 637 makes little difference to the spectra, since this compound has a very similar spectrum to that of titanomagnetite with $10Dq$ (O_h) = 1.8 eV (de Groot et al. 1990).

Based on this result and by allocating the cations in these titanomagnetite samples according to Table 6, the XMCD fit for Bushveld SA 637 and its composition ($Al_{0.12}Cr_{0.01}Mg_{0.08}Mn_{0.01}Ti_{0.37}V_{0.04}Fe_{2.10}\square_{0.27}O_4$) indicate n(A) = 0.84, n(B) = 1.89, and the data for Bushveld SA 620 ($Al_{0.12}Mg_{0.08}Mn_{0.01}Ti_{0.39}V_{0.02}Fe_{2.08}\square_{0.30}O_4$) gives n(A) = 0.80, n(B) = 1.90. The XMCD fit for Marangudzi T 203 and its composition ($Al_{0.12}Cr_{0.01}Mg_{0.02}Mn_{0.01}Ti_{0.14}V_{0.02}Fe_{2.64}\square_{0.04}O_4$) gives n(A) =0.92, n(B) = 2.04. These results show that the two Bushveld Ti-bearing spinels contain vacancies in the tetrahedral site as well as in the octahedral site while the Marangudzi sample only contains tetrahedral vacancies.

Lindsley (1976) discussed different cation substitution models for titanomagnetite (magnetite-ulvöspinel solid solution). For a stoichiometric metal/oxygen ratio, the Fe^{2+} and Fe^{3+} can be described, for $0 < x < 0.5$, according to the formula

$$(Fe^{3+})_A\ [Fe^{3+}_{1-2x}Fe^{2+}_{1+x}\ Ti^{4+}_x]_BO^{2-}_4 \quad (2)$$

However, the Fe^{2+} cations in the titanomagnetite are not thermodynamically stable and can oxidize to Fe^{3+} leading to the formation of titanomaghemite, which is the Ti-bearing analog of maghemite (γ-Fe_2O_3) (Perriat et al. 1999). Titanomaghemite is highly non-stoichiometric and end-member oxidized ulvöspinel would contain up to 2/3 cation vacancies per formula unit, compared to the 1/3 of γ-Fe_2O_3 (O'Reilly 1994). Equations 1 and 2 can be combined, and the presence of vacancies in the tetrahedral site (Δ) incorporated, to give a simplified equation describing oxidation of Ti-poor members of the magnetite-ulvöspinel series toward titanomaghemite, with $0 < x < 0.5$ and $0 < \delta < 0.33$

$$(Fe^{3+}_{1-\Delta}\square_\Delta)_A[Fe^{3+}_{1-2x+2\delta+\Delta}Fe^{2+}_{1+x-3\delta}\ Ti^{4+}_x\ \square_\delta]_BO^{2-}_4 \quad (3)$$

Equation 3 describes the oxidation of one Fe^{2+} to give compositions falling close to the oxidized ulvöspinel–maghemite join (γ-$FeTiO_3$–γ-Fe_2O_3) that is coincident with the ilmenite–hematite join (α-$FeTiO_3$–α-Fe_2O_3) (Fig. 9).

The magmatic spinel samples from Bushveld were presumably originally titanomagnetites. However XMCD results show that they are now highly oxidized with the vacancy values of around 0.28–0.30, indicating that they fall close to the oxidized ulvöspinel–maghemite join (Fig. 9). Figure 9 also demonstrates the shift in composition from the original stoichiometric, magmatic composition, which is likely to be represented by the microprobe analyses, recalculated on a 3 cation, 4 O atom basis. The Marangudzi sample is much less oxidized (less hydrothermally altered), and plots fairly close to the primary magnetite–ulvöspinel join at about the limit of equilibrium solid solution of the maghemite component in Ti-poor titanomagnetites (Senderov et al. 1993). The cell parameters for the Bushveld and Marangudzi samples (Table 3) support these observations. The presence of tetrahedral

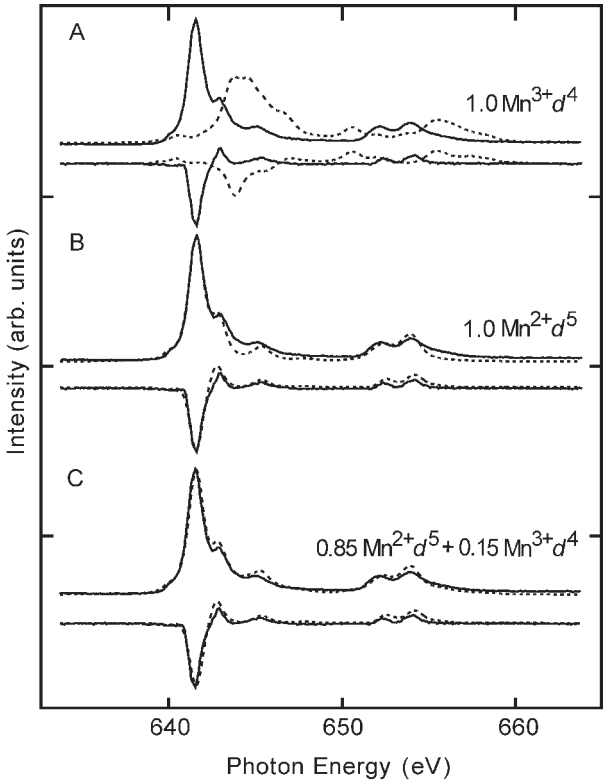

FIGURE 10. Mn $L_{2,3}$ XAS spectra. The calculated XMCD and isotrophic XAS spectra (dashed line), together with the experimental spectra for the Franklin ferrite (solid line) for (**a**) Mn^{3+} d^4 and (**b**) Mn^{2+} d^5 ground state in T_d symmetry, and (**c**) 85% Mn^{2+} d^5 and 15% Mn^{3+} d^4, (the Mn $L_{2,3}$ XAS spectra for both the Franklin and Långban ferrites are very similar).

site vacancies, the restriction of Ti^{4+} to the octahedral sites and the absence of tetrahedral Fe^{2+} were also noted by Collyer et al. (1988) in their study of a natural titanomaghemite crystal from the Bushveld complex. The extremely oxidized Bushveld titanomaghemites fall far outside the equilibrium titanomaghemite field (Senderov et al. 1993) and the existence of such metastable compositions reflects the absence of nucleation of the stable ilmenite-hematite phases during the post-magmatic cooling.

Cation-excess magnetites

The negative values for vacancies (Table 5) in the ferrite spinels from Långban and Franklin, which contain high concentrations of Mg and Zn, respectively, suggest that they contain an excess of cations ($Fe_{3+\delta}O_4$) compared with stoichiometric magnetite. Such high cation totals would be reduced if elements other than Fe are present in oxidation states higher than the divalent state assumed here, which is highly unlikely for Zn and Mg. However, there is some evidence to suggest that Mn could be present in higher oxidation states (Mn^{3+} and Mn^{4+}) in iron-manganese spinel oxides (Uzunova et al. 1998). To determine the oxidation state of Mn in these Mn-rich ferrites, the Mn *L*-edge XAS and XMCD spectra were obtained.

Calculated Mn $L_{2,3}$ absorption spectra were calculated using the crystal field atomic multiplet model described in van der Laan and Thole (1991) and van der Laan and Kirkman (1992) and the resulting spectra for Mn^{3+} d^4 and Mn^{2+} d^5 ground state in tetrahedral symmetry are shown in Figure 10, along with the spectra from the Franklin sample. In the calculation, a crystal field splitting of $10Dq = -0.6$ eV was included, together with a small magnetic field along the *z*-axis. This gives spectra quite similar to those for the atomic Mn d^4 ($^5D_4$) and Mn d^5 ($^6S_{5/2}$) ground state configurations. A larger crystal field parameter, common for octahedral sites, results in a distinct shoulder at the low energy side of the L_3 peak, whereas the measured spectrum only shows a small, hardly discernible feature. The small size of the crystal field for the Mn is a clear indication that the ion is in the tetrahedral site. The crystal field splitting is much smaller than for the octahedral site due to the larger atomic coordination resembling a more spherical surrounding. Indeed, Mn^{2+} and Zn^{2+} have a greater affinity for tetrahedral coordination than the Fe^{3+} ion, therefore the addition of Mn and/or Zn displaces the trivalent Fe from the tetrahedral to the octahedral sublattice. It is seen from the data in Table 4 that the presence of the Mn^{2+} in Långban and Franklin leads to a decrease in the Fe^{2+}/Fe^{3+} ratio for the octahedral site to maintain the charge balance. Although the calculated Mn^{2+} d^5 spectrum fits the measured data rather well, there is an intensity deficit at the high-energy sites of the L_3 and L_2 edges (Fig. 10b). As is seen in Figure 10c, the fit of the XAS is significantly improved by including 15% Mn^{3+} d^4. A further indication for a predominant d^5 character stems from the large branching ratio, $L_3/(L_2 + L_3)$, in XAS that reveals a high-spin $S = 5/2$ state (Thole and van der Laan 1988). Thus, the comparison with the calculations shows that ~85% of Mn is Mn^{2+} (d^5) with ~15% as Mn^{3+} (d^4). This is in agreement with the results of Hastings and Corliss (1956) who reported that 80% of the Mn in $MnFe_2O_4$ occupies the T_d sublattice (Smit and Wijn 1959). Their results were derived using neutron diffraction, which provides reliable occupation parameters due to the significant difference (magnitude and sign) in the scattering lengths of Fe and Mn.

Figure 10 also shows the calculated XMCD (van der Laan and Thole 1991). Similar results have also been reported by Stichauer et al. (2001). We see that for a pure d^5 ground state the agreement is already quite good (Fig. 10b) and that including 15% Mn d^4 gives no noticeable improvement (Fig. 10c). Better agreement is probably beyond the reach of the atomic calculations. We find experimentally from the signs of the measured XMCD that the Mn moment is parallel to that of the Fe tetrahedral sublattice moments, which is another indication that Mn is in the tetrahedral site. The magnitude of the XMCD for the franklinite corresponds to a magnetic moment of about -3 μ_B per Mn atom, which is smaller than the saturation value of -5 μ_B because the 0.6 Tesla field is not sufficient to saturate the grains oriented in arbitrary directions.

As the non-stoichiometry in the Franklin and Långban samples cannot be fully accounted for by the presence of cations in higher oxidation states, it seems likely that these spinels do contain an excess of cations. The Franklin and Långban ferrite spinels show substantial amounts of other elements substituted for Fe, therefore they no longer resemble the model Fe_3O_4 system on which the fitting procedures and calculations are based. Thus, the absolute errors in these more complex spinels may be larger than those previously stated (±0.01 atoms). It is significant that

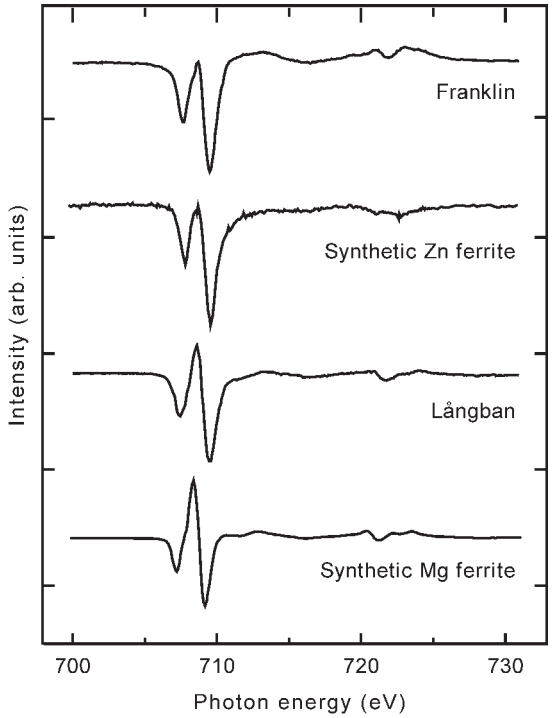

FIGURE 11. The experimentally derived Fe XMCD spectra of natural cation-excess magnetites from Franklin ($Al_{0.03}Mg_{0.02}Mn_{0.33}Zn_{0.45}Fe_{2.21}O_4$) and Långban ($Al_{0.03}Mg_{0.80}Mn_{0.15}Zn_{0.02}Fe_{2.05}O_4$). Note the similar XMCD spectra for these natural samples compared to those for the corresponding synthetic end-member Zn spinel ferrite ($Mn_{0.01}Zn_{0.67}Fe_{2.36}O_4$) and Mg spinel ferrite ($Mg_{0.95}Mn_{0.01}Fe_{2.09}O_4$) from Pattrick et al. (2002).

the Franklin and Långban ferrite spinels, the only two natural samples exhibiting an excess of cations, are rich in zinc and manganese, respectively, because synthetic cation-excess ferrite spinels reported in the literature commonly involve Zn^{2+}- or Mn^{2+}-bearing components (Tamaura and Tabata 1990; Tabata et al. 1993, 1994; Togawa et al. 1996). Cation-excess magnetite has also been observed from the reduction of hematite to magnetite at one atmosphere and high temperatures (Betancur et al. 2003). Note that in some of these studies (Tabata et al. 1993, 1994), the non-stoichiometric ferrite spinels are referred to as being oxygen-deficient, with the formula $Fe_3O_{4-\delta}$, rather than cation-excess.

Very few reports on natural oxygen-deficient (cation-excess) magnetites are available and their occurrence at Långban, Sweden, and Franklin, U.S.A. is unusual. Chemical, mineralogical, and isotope analysis of ores from Långban and Franklin suggest that these deposits were formed, in a similar manner as exhalative-sedimentary ores (Boström et al. 1979). It seems that the entry of significant proportions of Mg, Zn, and Mn into the spinel structure stabilizes cation excess (oxygen-poor) varieties, but it is also conceivable that this method of formation might have resulted in oxygen being removed from the spinel structure.

The XMCD spectra obtained for the Långban and Franklin magnetites are very similar to those obtained for the synthetic magnesium end-member ($Mg_{0.95}Mn_{0.01}Fe_{2.09}$) and zinc end-member ($Mn_{0.01}Zn_{0.67}Fe_{2.36}$), respectively (Fig. 11). Iron site occupancies of 0.19 Fe d^6O_h, 0.75 Fe d^5T_d, and 1.11 d^5O_h (Table 4) were obtained for the Långban magnesioferrite ($Al_{0.03}Mg_{0.80}Mn_{0.15}Zn_{0.02}Fe_{2.05}O_4$), showing that Mg predominately replaces Fe^{2+} in the B site, with approximately 10% allocated to the A site. This Mg distribution is in agreement with the conclusions of O'Neill et al. (1992). Incorporating the non-Fe cations as described in Table 6, site occupancies of n(A) = 1.00, n(B) = 2.05 were obtained, with the cation excess in the octahedral site. This distribution is identical to that obtained for the synthetic magnesioferrite ($Mg_{0.95}Mn_{0.01}Fe_{2.09}$) when the spinel composition is calculated from EPMA and XMCD data. In this case, 0.1 atoms pfu of the total Mg content (0.95 atoms pfu) are required to fill the A site.

It is generally believed that Zn^{2+} has a stronger preference for occupation of the A site than any other ion, including Fe^{3+}. Iron site occupancies of 0.39 Fe d^6O_h, 0.62 Fe d^5T_d, and 1.20 d^5O_h (Table 4) were obtained for the Franklin zinc-rich magnetite ($Al_{0.03}Mg_{0.02}Mn_{0.33}Zn_{0.45}Fe_{2.21}O_4$). After allocation of 85% of the Mn to the A site, only 0.1 atoms pfu of Zn are required to fill this site, leaving 0.35 atoms of Zn to enter the B site. A similar distribution was also obtained for the synthetic zinc spinel ($Mn_{0.01}Zn_{0.67}Fe_{2.36}$) (Table 4). For this sample only 0.38 atoms pfu Zn are required to fill the A site leaving 0.29 atoms to enter the B site. These results suggest that up to 78% of the Zn in these Zn-rich ferrite spinels is present in the B site rather than a maximum value of 19% as suggested by earlier work on ferrite spinels (O'Neill 1992). Note that allocation of 81% of the available Zn to the tetrahedral site would give occupancies of n(A) = 1.26, n(B) = 1.78 for Franklin, and n(A) = 1.16, n(B) = 1.88 for the synthetic zinc spinel . This combination of large cation excesses in the A site with similarly large deficiencies in the B site seems unlikely. Thus, the former allocation is preferred, which gives occupancies of n(A) = 1.00, n(B) = 2.04, with a small cation excess in the octahedral site. This is in good agreement with the results found here for the natural and synthetic Mg-rich ferrite spinels, which also have an excess of cations over 3.0 atoms pfu.

ACKNOWLEDGMENTS

We thank V.S. Coker for discussions about the XMCD results and in particular for her work on the figures. We thank I. Kirkman for developing the CFIT program and for the help on Beamline 1.1. We are indebted to D.A. Plant for his assistance with the electron microprobe analysis. We also acknowledge the contribution of N.D. Telling in the later part of this study and to Don Lindsley for explaining some spinel crystal chemical subtleties to us.

REFERENCES CITED

Barker, D.S. (1995) Crystallization and alteration of quartz monzonite, Iron Springs mining district, Utah: relation to associated iron deposits. Economic Geology and the Bulletin of the Society of Economic Geologists, 90, 2197–2217.

Betancur, J.D., Restrepo, J., Palacio, C.A., Morales, A.L., Mazo-Zuluaga, J., Fernández, J.J., Pérez, O., Valderruten, J.F., and Bohórquez, A. (2003) Thermally driven and ball-milled hematite to magnetite transformation. Hyperfine Transactions, 148/149, 163–175.

Boström, K., Rydell, H., and Joensuu, O. (1979) Långban—An exhalative sedimentary deposit? Economic Geology, 74, 1002–1011.

Brice-Profeta, S. (2004) Étude de l'ordre chimique et magnétique d'oxydes spinelles de taille nanométrique par dichroïsme magnétique circulaire des rayons X. École doctorale Physique et Chimie des Matériaux. Ph.D. Thesis, Université Pierre et Marie Curie, Paris.

Buddington, A.F. and Lindsley, D.H. (1964) Iron-titanium oxide minerals and synthetic equivalents. Journal of Petrology, 5, 310–357.

Burns, R.G. (1993) Mineralogical applications of crystal field theory. Cambridge University Press, Cambridge.

Carbonin, S., Russo, U., and Della Giusta, A. (1996) Cation distribution in some natural spinels from X-ray diffraction and Mössbauer spectroscopy. Mineral-

ogical Magazine, 60, 355–368.
Chen, C.T., Idzerda, Y.U., Lin, H.J., Smith, N.V., Meigs, G., Chaban, E., Ho, G.H., Pellegrin, E., and Sette, F. (1995) Experimental confirmation of X-ray magnetic circular dichroism, sum-rules for iron and cobalt. Physical Review Letters, 75, 152–155.
Chen, J., Huang, D.J., Tanaka, A., Chang, C.F., Chung, S.C., Wu, W.B., and Chen, C.T. (2004) Magnetic circular dichroism in Fe 2*p* resonant photoemission of magnetite. Physical Review B, 69, 085107-1–085107-8.
Coey, J.M.D., Berkowits, A.E., Balcells, L.I., Putris, F.F., and Parker, F.T. (1998) Magnetoresistance of magnetite. Applied Physics Letters, 72, 734–736.
Collyer, S., Grimes, N.W., Vaughan, D.J., and Longworth, G. (1988) Studies of the crystal structure and crystal chemistry of titanomaghemite. American Mineralogist, 73, 153–160.
Cornell, R.M. and Schwertmann, U. (2003) The iron oxides. Structure, properties, reactions, occurrences and uses. Wiley-VCH, Weinheim.
Cowan, R.D. (1981) The theory of atomic structure and spectra, 16, p. 456–484. University of California Press, Berkeley.
Cox, K.G., Johnson, R.L., Monkman, L.J., Stillman, C.J., Vail, J.R., and Wood, D.N. (1965) The geology of the Nuanestsi province. Philosophical Transactions of the Royal Society, Series A, 257, 71–218.
Cressey, G., Henderson, C.M.B., and van der Laan, G. (1993) Use of *L*-edge X-ray absorption spectroscopy to characterize multiple valence states of *3d* transition metals; a new probe for mineralogical and geochemical research. Physics and Chemistry of Minerals, 20, 111–119.
de Castro, A.R.B., Fonesca, P.T., Pacheco, J.G., da Silva, J.C.V., and Santana, M.H.A. (2001) *L*-edge inner shell spectroscopy of nanostructured Fe_3O_4. Journal of Magnetism and Magnetic Materials, 233, 69–73.
de Groot, F.M.F., Fuggle, J.C., Thole, B.T., and Sawatzky, G.A. (1990) $L_{2,3}$ X-ray absorption edges of d° compounds: K^+, Ca^{2+}, Sc^{3+}, and Ti^{4+} in O_h (octahedral) symmetry. Physical Review B, 41, 928.
Droop, G. (1984) A general equation for estimating Fe^{3+} concentrations in ferromagnesian silicates and oxides from microprobe analyses, using stoichiometric criteria. Mineralogical Magazine, 51, 431–435.
Dudzik, E., van der Laan, G., and Thompson, S.M. (2000) Flipper—a new instrument for XMCD at the SRS. Synchrotron Radiation News, 13(4), 18–22.
Frost, B.R. (1991a) Introduction to oxygen fugacity and its petrologic importance. In D.H. Lindsley, Ed., Oxide minerals: petrologic and magnetic significance, 25, p. 1–9. Reviews in Mineralogy, Mineralogical Society of America, Chantilly, Virginia.
——— (1991b) Stability of oxide minerals in metamorphic rocks. In D.H. Lindsley, Ed., Oxide minerals: petrologic and magnetic significance, 25, p. 469–487. Reviews in Mineralogy, Mineralogical Society of America, Chantilly, Virginia.
Gillot, B. (1994) Infrared spectrometric investigation of submicron metastable cation-deficient spinels in relation to order-disorder phenomena and phase transition. Vibrational Spectroscopy, 6, 127–148.
Goodenough, J.B. and Loeb, A.L. (1955) Theory of ionic ordering, crystal distortion, and magnetic exchange due to covalent forces in spinels. Physical Review, 98, 391–408.
Goss, C.J. (1988) Saturation magnetisation, coercivity and lattice parameter changes in the system Fe_3O_4-γ-Fe_2O_3, and their relationship to structure. Physics and Chemistry of Minerals, 16, 164–171.
Harney, D.M.W. and von Gruenewaldt, G. (1995) Ore-forming processes in the upper part of the Bushveld complex, South Africa. Journal of African Earth Sciences, 20(2), 77–89.
Hastings, J.M. and Corliss, L.M. (1956) Neutron diffraction study of manganese ferrite. Physical Review, 104, 328–331.
Henderson, C.M.B., Cressey, G., and Redfern, S.A.T. (1994) Geological applications of synchrotron radiation. Radiation Physics and Chemistry, 45, 459–481.
Hochepied, J.F., Sainctavit, P., and Pileni, M.P. (2001) X-ray absorption spectra and X-ray magnetic circular dichroism studies at Fe and Co $L_{2,3}$ edges of mixed cobalt-zinc ferrite nanoparticles: cationic repartition, magnetic structure and hysteresis cycles. Journal of Magnetism and Magnetic Materials, 231, 315–322.
Holland, T.J.B. and Redfern, S.A.T. (1997) Unit-cell refinement from powder diffraction data: The use of regression diagnostics. Mineralogical Magazine, 61, 65–77.
Hossain, M.T. (1970) Petrology and mineralogy of the Marangudzi ring complex, Rhodesia. Ph.D. thesis, University of Manchester.
Hossain, M.T. and Henderson, C.M.B. (1977) Gabbros of Marangudzi Complex, Zimbabwe. Journal of Mining Geology, 14(1), 1–15.
Huang, D.J., Chang, C.F., Jeng, H.-T., Guo, G.Y., Lin, H.-J., Wu, W.B., Ku, H.C., Fujimori, A., Takahashi, Y., and Chen, C.T. (2004) Spin and orbital magnetic moments of Fe_3O_4. Physical Review Letters, 93, 077204/1–4.
Kuiper, P., Searle, B.G., Duda, L.-C., Wolf, R.M., and van der Zaag, P.J. (1997) Fe $L_{2,3}$ linear and circular magnetic dichroism of Fe_3O_4. Journal of Electron Spectroscopy and Related Phenomena, 86, 107–113.
Lindsley, D.H. (1976) The Crystal Chemistry and Structure of Oxide Minerals as Exemplified by the Fe-Ti Oxides. In D. Rumble, Ed., Mineralogical Society of America: Short Course Notes, 3, p. L-1–60. Mineralogical Society of America, Chantilly, Virginia.
——— Ed. (1991) Oxide minerals: petrologic and magnetic significance, 25. Reviews in Mineralogy, Mineralogical Society of America, Chantilly, Virginia.
Lu, Y.X., Claydon, J.S., Xu, Y.B., Thompson, S.M., Wilson, K., and van der Laan, G. (2004) Epitaxial growth and magnetic properties of half-metallic Fe_3O_4 on GaAs(100). Physical Review B, 70, 233304/1–4.
Lucchesi, S., Russo, U., and Della Giusta, A. (1999) Cation distribution in natural Zn-spinels: franklinite. European Journal of Mineralogy, 11, 501–511.
Morrall, P., Schedin, F., Case, G.S., Thomas, M.F., Dudzik, E., van der Laan, G., and Thornton, G. (2003) Stoichiometry of $Fe_{3-\delta}O_4$(111) ultrathin films on Pt(111). Physical Review B, 67, 214408-1–214408-7.
O'Neill, H.St.C. (1992) Temperature dependence of the cation distribution in zinc ferrite ($ZnFe_2O_4$) from powder XRD structural refinements. European Journal of Mineralogy, 4, 571–580.
O'Neill, H.St.C., Annersten, H., and Virgo, D. (1992) The temperature dependence of the cation distribution in magnesioferrite ($MgFe_2O_4$) from powder XRD structural refinements and Mössbauer spectroscopy. American Mineralogist, 77, 725–740.
O'Reilly, W. (1994) Magnetic recording in nature: the medium, the mechanism and the message. Journal of Magnetism and Magnetic Materials, 137, 167–185.
Pattrick, R.A.D., van der Laan, G., Henderson, C.M.B., Kuiper, P., Dudzik, E., and Vaughan, D.J. (2002) Cation site occupancy in spinel ferrites studied by X-ray magnetic circular dichroism: developing a method for mineralogists. European Journal of Mineralogy, 14, 1095–1102.
Pellegrin, E., Hagelstein, M., Doyle, S., Moser, H.O., Fuchs, J., Vollath, D., Schuppler, S., James, M.A., Saxena, S.S., Nielsen, L., Rogojanu, O., Sawatzky, G.A., Ferrero, C., Borowski, M., Tjernberg, O., and Brookes, N. (1999) Characterization of nanocrystalline γ-Fe_3O_4 with synchrotron radiation techniques. Physica Status Solidi B, 215, 797–801.
Perriat, P., Fries, E., Millot, N., and Domenichini, B. (1999) XPS and EELS investigation of chemical homogeneity in nanometer scaled Ti-ferrites obtained by soft chemistry. Solid State Ionics, 117, 175–184.
Roelofsen, J.N., Peterson, R.C., and Raudsepp, M. (1992) Structural variation in nickel aluminate spinels ($NiAl_2O_4$). American Mineralogist, 77, 522–528.
Schedin, F., Morrall, P., Petrov, V.N., Case, S., Thomas, M.F., Dudzik, E., van der Laan, G., and Thornton, G. (2000) Magnetic properties of ultrathin epitaxial Fe_3O_4 films on Pt(111). Journal of Magnetism and Magnetic Materials, 211, 266–270.
Schedin, F., Hill, E.W., van der Laan, G., and Thornton, G. (2004) Magnetic properties of stoichiometric and nonstoichiometric ultrathin Fe_3O_4(111) films on Al_2O_3(0001). Journal of Applied Physics, 96, 1165–1169.
Schofield, P.F., Henderson, C.M.B., Cressey, G., and van der Laan, G. (1995) 2*p* X-ray absorption spectroscopy in the Earth Sciences. Journal of Synchrotron Radiation, 2, 93–98.
Schütz, G., Fischer, P., Goering, E., Attenkofer, K., Ahlers, D., and Röbl, W. (1997) X-ray magnetic circular dichroism. Synchrotron Radiation News, 10(4), 13–26.
Senderov, E., Dogan, A.U., and Navrotsky, A. (1993) Nonstoichiometry of magnetite-ulvöspinel solid solutions quenched from 1300 °C. American Mineralogist, 78, 565–573.
Sette, F., Chen, C.T., Ma, Y., Modesti, S., and Smith, N.V. (1990) Magnetic circular dichroism studies with soft X-rays. X-ray and inner shell processes, 215, p. 96–105. AIP, New York.
Shannon, R.D. (1976) Revised effective ionic radii and systematic studies of interatomic distances in halides and chalcogenides. Acta Crystallographica, A32, 751–767.
Smit, J. and Wijn, H.P.J. (1959) Ferrites. Physical properties of ferrimagnetic oxides in relation to their technical applications. Wiley, New York.
Steers, J.E. (2003) Extracts from Balmat Mine Resources and reserve Audit, January 2003. http://instruct.uwo.ca/earth-sci/fieldlog/Grenville/balmat.htm
Stichauer, L., Mirone, A., Turchini, S., Prosperi, T., Zennaro, S., Zema, N., Lama, F., Potin, R., Simsa, Z., Tailhades, P., and Bonningue, C. (2001) X-ray absorption spectroscopy and magnetic circular dichroism of the Mn-ferrite nanocrystalline thin films. Journal of Applied Physics, 90, 2511–2516.
Stöhr, J. (1995) X-ray magnetic circular dichroism spectroscopy of transition metal thin films. Journal of Electron Spectroscopy and Related Phenomena, 75, 253–272.
Tabata, M., Nishida, Y., Kodama, T., Mimori, K., Yoshida, T., and Tamaura, Y. (1993) CO_2 decomposition with oxygen-deficient Mn(II) ferrite. Journal of Materials Science, 28, 971–974.
Tabata, M., Akanuma, K., Togawa, T., Tsuji, M., and Tamaura, Y. (1994) Mössbauer study of oxygen-deficient ZnII-bearing ferrites ($Zn_xFe_{3-x}O_{4-\delta}$, 0 = x = 1) and their reactivity toward CO_2 decomposition to carbon. Journal of the Chemical Society Faraday Transactions, 90, 1171–1175.
Tamaura, Y. and Tabata, M. (1990) Complete reduction of carbon dioxide to carbon using cation-excess magnetite. Nature, 346, 255–256.
Thole, B.T. and van der Laan, G. (1988) Branching ratio in X-ray absorption spectroscopy. Physical Review B, 38, 3158–3171.

Thole, B.T., Cowan, R.D., Sawatzky, G.A., Fink, J., and Fuggle, J.C. (1985) New probe for the ground-state electronic structure of narrow-band and impurity systems. Physical Review B, 31, 6856–6858.

Thole, B.T., Carra, P., Sette, F., and van der Laan, G. (1992) X-ray circular dichroism as a probe of orbital magnetization. Physical Review Letters, 68, 1943–1946.

Togawa, T., Sano, T., Wada, Y., Yamamoto, T., Tsuji, M., and Tamaura, Y. (1996) The effect of the crystal orientation of the rate of formation of cation-excess magnetite. Solid State Ionics, 89, 279–286.

Uzunova, E.L., Klissurski, D.G., and Namska, S.D. (1998) Surface studies of nano-dimensional particles size iron-manganese spinel mixed oxides. Canadian Journal of Chemistry, 76, 1361–1364.

van der Laan, G. (1990) Polaronic satellites in X-ray absorption spectra. Physical Review B, 41, 12366–12368.

van der Laan, G. and Kirkman, I.W. (1992) The 2*p* absorption spectra of 3*d* transition metal compounds in tetrahedral and octahedral symmetry. Journal of Physics: Condensed Matter, 4, 4189–4204.

van der Laan, G. and Thole, B.T. (1988) Angular dependent photoelectron yield. Measurement of the La 3*d* Auger and autoionization life time width. Journal of Electron Spectroscopy and Related Phenomena, 46, 123–129.

——— (1991) Strong magnetic X-ray dichroism in 2*p* absorption spectra of 3*d* transition metal ions. Physical Review B, 43, 13401–13411.

van der Laan, G., Thole, B.T., Sawatzky, G.A., Goedkoop, J.B., Fuggle, J.C., Esteva, J.M., Karnatak, R.C., Remeika, J.P., and Dabkowska, H.A. (1986a) Experimental proof of magnetic X-ray dichroism. Physical Review B, 34, 6529–6531.

van der Laan, G., Zaanen, J., Sawatzky, G.A., Karnatak, R.C., and Esteva, J.M. (1986b) Comparison of X-ray absorption with X-ray photoemission of nickel dihalides and NiO. Physical Review B, 33, (4253–4263).

van der Laan, G., Henderson, C.M.B., Pattrick, R.A.D., Dhesi, S.S., Schofield, P.F., Dudzik, E., and Vaughan, D.J. (1999) Orbital polarization in $NiFe_2O_4$ measured by Ni 2*p* X-ray magnetic circular dichroism. Physical Review B, 59, 4314–4321.

Waychunas, G.A. (1991) Crystal chemistry of oxides and oxyhydroxides. In D.H. Lindsley, Ed., Oxide minerals: petrologic and magnetic significance, 25, p. 11–68. Reviews in Mineralogy, Mineralogical Society of America, Chantilly, Virginia.

Wright, J.P., Attfield, J.P., and Radaelli, P.G. (2001) Long range charge ordering in magnetite below the Verwey transition. Physical Review Letters, 27, 266401/1–4.

Yamanaka, T. and Okita, M. (2001) Magnetic properties of the Fe_2SiO_4-Fe_3O_4 spinel solid solutions. Physics and Chemistry of Minerals, 28, 102–109.

MANUSCRIPT RECEIVED JULY 29, 2005
MANUSCRIPT ACCEPTED JANUARY 18, 2006
MANUSCRIPT HANDLED BY G. DIEGO GATTA